Front. Optoelectron. 2021, 14(2): 154–169
https://doi.org/10.1007/s12200-021-1125-4

REVIEW ARTICLE

Magnetically controllable metasurface and its application

Yu BI[1], Lingling HUANG (✉)[1], Xiaowei LI[2], Yongtian WANG[1]

1 Key Laboratory of Photoelectronic Imaging Technology and System, Ministry of Education; School of Optics and Photonics, Beijing Institute of Technology, Beijing 100081, China
2 Laser Micro/Nano-Fabrication Laboratory, School of Mechanical Engineering, Beijing Institute of Technology, Beijing 100081, China

Abstract The dynamic control of the metasurface opens up a vital technological approach for the development of multifunctional integrated optical devices. The magnetic field manipulation has the advantages of sub-nanosecond ultra-fast response, non-contact, and continuous adjustment. Thus, the magnetically controllable metasurface has attracted significant attention in recent years. This study introduces the basic principles of the Faraday and Kerr effect of magneto-optical (MO) materials. It classifies the typical MO materials according to their properties. It also summarizes the physical mechanism of different MO metasurfaces that combine the MO effect with plasmonic or dielectric resonance. Besides, their applications in the nonreciprocal device and MO sensing are demonstrated. The future perspectives and challenges of the research on MO metasurfaces are discussed.

Keywords magneto-optical (MO) effect, MO metasurfaces, magnetoplasmonic, nonreciprocal device, MO sensing

1 Introduction

Metasurface is a two-dimensional (2D) subwavelength artificial micro-nano structure that can realize flexible control of electromagnetic wave's amplitude, phase, polarization, propagation, and other characteristics [1–6]. However, most metasurfaces can only achieve specific functions due to the limitation of fixed structure. By integrating functional materials with variable properties induced by external excitation, tunable metasurface can be achieved. Currently, the methods of realizing active metasurface mainly include mechanical [7], thermal [8–10], electrical [11], optical [12], and magnetic [13] control, and so on. Among them, magnetic field manipulation becomes a very promising way due to its advantages of sub-nanosecond ultra-fast response, non-contact, and continuous adjustment. Magneto-optical (MO) material is a kind of functional material, whose non-diagonal element of the permittivity tensor change from zero to a variable once an external magnetic field is applied. It is the origin that the MO effect occurs. Therefore, light field manipulation by magnetic control can be achieved by introducing MO materials into the metasurface.

The MO effects mainly refer to Faraday, Kerr, Zeeman, and magneto-birefringence. Among them, Faraday and Kerr effects are widely combined with metasurfaces. The MO phenomenon stems from different propagation rates and absorption of left-handed and right-handed circularly polarized light passing through magnetic materials. While a linearly polarized light is incident on a magnetized MO medium, the orthogonal circularly polarized light can produce a phase and amplitude difference, leading the transmitted (Faraday effect) or reflected light (Kerr effect) to become elliptically polarized and the rotation of polarization. It is worth noting that Faraday effect has a unique property of breaking the time-reversal symmetry and Lorentz reciprocity, making it applicable to various nonreciprocal devices, such as isolators and circulators. MO metasurfaces based on Faraday and Kerr effects have been widely used in various fields, such as chiral sensing [14], biochemical sensing [15], magnetic field sensing [16], MO storage [17], and MO switch [18]. However, it is challenging to make the nanoscale metasurface achieve a strong response due to the weak effect of the MO material. To overcome this problem, researchers have attempted to combine the magnetoplasmonic or dielectric resonance with nanostructures.

In this review, we summarize the physical mechanism, structural design, and application of the MO metasurfaces. We describe the propagation of light waves in MO materials and the theoretical principle of Faraday and Kerr effects in the first part. Then, we introduce the typical

Received November 15, 2020; accepted January 19, 2021

E-mail: huanglingling@bit.edu.cn

MO materials and classify them by material properties. We classify the MO nanostructures according to the material composition, such as ferromagnetic metal (FM), noble metal (NM)-FM, ferromagnetic dielectric-NM, FM-dielectric, and all-dielectric material. Besides, we discuss the corresponding working principles of realizing the magnetically controlled optical field. Finally, we present an outlook on some promising areas of MO metasurfaces.

2 Fundamentals of magneto-optical effect

2.1 Light propagation in magneto-optical materials

The physical origin of MO effect in magnetized medium is caused by the change of the off-diagonal element of its dielectric tensor. In this section, we discuss the evolution of an electromagnetic wave inside the medium starting from the Maxwell equations and constitutive relations.

In the case of no sources, the Maxwell equations and constitutive relation can be expressed as

$$\nabla \times \vec{E} = \frac{\partial \vec{D}}{\partial t}, \tag{1}$$

$$\nabla \times \vec{H} = \frac{\partial \vec{B}}{\partial t}, \tag{2}$$

$$\nabla \cdot \vec{D} = 0, \tag{3}$$

$$\nabla \cdot \vec{B} = 0, \tag{4}$$

$$\vec{D} = \varepsilon_0 \tilde{\varepsilon} \vec{E}, \tag{5}$$

$$\vec{B} = \mu_0 \tilde{\mu} \vec{H}, \tag{6}$$

where $\vec{E}$ is the electric field, $\vec{D}$ is the electric displacement vector, $\vec{B}$ is the magnetic induction, $\vec{H}$ is the magnetic field, ε_0 and μ_0 denote the vacuum permittivity and permeability, respectively, $\tilde{\varepsilon}$ and $\tilde{\mu}$ denote the relative permittivity and permeability of the medium, respectively. At optical frequency, it is assumed that $\mu = 1$. Assuming that the incident light is a plane wave, the Helmholtz equation is derived as

$$\left(k^2 \delta_{ij} - \frac{\omega^2}{c^2} \tilde{\varepsilon}\right) \cdot \vec{E} = 0, \tag{7}$$

where δ_{ij} is the identity matrix (for $i = j$, $\delta_{ij} = 1$; for $i \neq j$, $\delta_{ij} = 0$), k is the wave vector, ω is the angular frequency, and c is the speed of light in the vacuum. When Eq. (7) satisfies

$$\det\left|k^2 \delta_{ij} - \frac{\omega^2}{c^2} \varepsilon_{ij}\right| = 0, \tag{8}$$

where ε_{ij} is the component of the relative permittivity tensor $\tilde{\varepsilon}$, there exists a nontrivial solution. Assuming that the external magnetic field is along the z-axis, the dielectric tensor can be expressed as

$$\tilde{\varepsilon} = \begin{pmatrix} \varepsilon_x & -\mathrm{i}g & 0 \\ \mathrm{i}g & \varepsilon_y & 0 \\ 0 & 0 & \varepsilon_z \end{pmatrix}, \tag{9}$$

where g is the gyration coefficient, which is related to the applied magnetic field. Using the refractive index $n = \frac{c}{w}|k|$, we obtain the wave vectors as follows

$$k_{\pm} = \frac{\omega}{c} \sqrt{\varepsilon_x \pm g} = \frac{\omega}{c} n_{\pm}. \tag{10}$$

Substituting Eq. (10) into Eq. (7), then the electric field can be expressed as

$$\vec{E}_{\pm} = \frac{E_0}{2} \mathrm{e}^{[\mathrm{i}(k_{\pm} z - \omega t)]} (\hat{e}_x + \hat{e}_y \mathrm{e}^{\mathrm{i}(\pm \frac{\pi}{2})}). \tag{11}$$

Thus, the eigenmodes of the orthogonal circularly polarized electromagnetic waves can be obtained with different phase velocities $c_{\pm} = c/n_{\pm}$.

2.2 Faraday effect

The Faraday effect refers to the optical phenomenon of polarization rotation for the transmitted light. Specifically, when a linearly polarized light is incident into a MO medium perpendicularly and the applied magnetic field is parallel to the light propagation, the transmitted light is transformed into the elliptically polarized after passing through the medium, and the polarization plane rotates at a certain angle, as shown in Fig. 1.

Assuming that the x-polarized incident light propagates along the z-axis, which is parallel to the external magnetic field, the incident electric field can be expressed as a linear combination of two eigenmodes

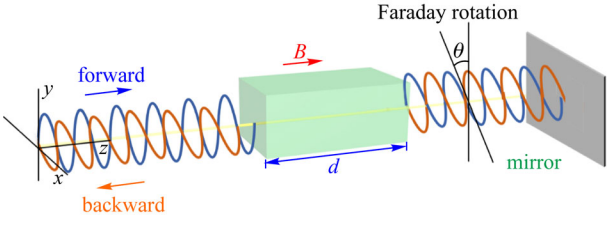

Fig. 1 Schematic of the Faraday effect

$$E_i = E_0\hat{e}_x e^{[i(kz-\omega t)]} = \frac{E_0}{2}e^{[i(kz-\omega t)]}(\hat{e}_x + \hat{e}_y e^{-i\frac{\pi}{2}})$$

$$+\frac{E_0}{2}e^{[i(kz-\omega t)]}(\hat{e}_x + \hat{e}_y e^{i\frac{\pi}{2}}). \quad (12)$$

According to the Fresnel equation, the transmission coefficient at the interface of the two media n_1 and n_2 is given as

$$t = \frac{2n_1}{n_1 + n_2}. \quad (13)$$

Then, the transmitted electric field is given by

$$E_t = \frac{2n_1}{n_1 + n_+}E_+ + \frac{2n_1}{n_1 + n_-}E_-$$

$$\approx \frac{2}{1 + \frac{n_+ + n_-}{2}}(E_+ + E_-) = A(E_+ + E_-). \quad (14)$$

When the light wave propagates a distance d in the medium, we obtain the phase difference of the orthogonal circularly polarized light and the corresponding electric field as follows

$$\Delta f = k_+ d - k_- d = \frac{\omega}{c}(n_+ - n_-)d = \frac{\omega}{c}\frac{g}{\sqrt{\varepsilon_x}}d, \quad (15)$$

$$E(d) = A\Big(E_+(d) + E_-(d)\Big)$$

$$= AE_0\begin{pmatrix}\cos\left(\frac{\Delta f}{2}\right)\\ \sin\left(\frac{\Delta f}{2}\right)\end{pmatrix}e^{[-i\omega(t-c^{-1}n_0 d)]}. \quad (16)$$

It can be seen that the linearly polarized light is transformed into the elliptically polarized due to the produced phase difference after passing through the medium. The polarization plane is rotated by a certain angle. The Faraday rotation angle and the ellipticity can be expressed as

$$\theta_F = \mathrm{Re}\left\{\frac{\Delta f}{2}\right\} = \frac{\omega}{2c}\mathrm{Re}\left\{\frac{g}{\sqrt{\varepsilon_x}}\right\}d, \quad (17)$$

$$\Psi_F = \mathrm{Im}\left\{\frac{\Delta f}{2}\right\} = \frac{\omega}{2c}\mathrm{Im}\left\{\frac{g}{\sqrt{\varepsilon_x}}\right\}d. \quad (18)$$

In general, the Faraday rotation can be expressed as

$$\theta = VBd, \quad (19)$$

where V is the Verdet constant of the MO material. It is determined by the dielectric properties and the wavelength of the incident light. And it characterizes the MO properties of the material. If the material is ferromagnetic or ferrimagnetic, the relationship between B and θ is not linear while the magnetic saturation occurs. In this case, the rotation angle per unit length of the material at saturation magnetization is used to characterize the strength of the Faraday effect. In addition, from Eqs. (17) and (18), the Faraday rotation and ellipticity are respectively related to the real and imaginary part of the gyration coefficient g.

Importantly, the unique property of the Faraday effect is that it can break the time-reversal symmetry and Lorentz reciprocity. Thus, the polarization rotation is not determined by the propagation of the light wave but by the direction of the external magnetic field. This property can be applied to nonreciprocal devices, such as MO isolator or circulator.

2.3 Kerr effect

The MO Kerr effect (MOKE) refers to the phenomenon that the polarization and intensity of the reflected light change after a linearly polarized light is incident on the surface of the magnetized medium. The MOKE can be observed in both transparent and opaque materials since it mainly depends on the reflective properties of the medium. The polarization rotation mainly depends on the off-diagonal element of the dielectric tensor. Based on the relative relationship between the magnetization, the incident plane, and the material surface, the MOKE is classified into three types: polar, longitudinal, and transversal MOKE, as shown in Fig. 2.

When the sample is placed in a magnetic field, the electrons in the magnetized medium oscillate under the action of light waves and move vertically to the magnetic field due to the Lorentz force. It makes the p-polarization (TM wave) and s-polarization (TE wave) interconvert. For PMOKE (the magnetization is perpendicular to the material surface and parallel to the incident plane) and LMOKE (the magnetization is parallel to the incident plane), the reflected light becomes elliptically polarized. While for TMOKE (the magnetization is parallel to the material surface and perpendicular to the incident plane), the polarization of the reflected light has not changed, but its intensity has.

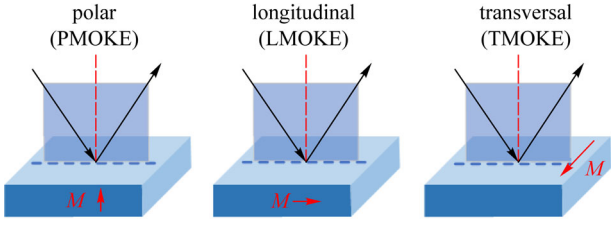

Fig. 2 Schematic of MOKE

The polarization rotation and ellipticity of the PMOKE are given as follows, respectively.

$$\theta_{\mathrm{p}} = \mathrm{Im}\frac{\eta^2[\sqrt{\eta^2-\sin^2\theta} \mp \sin\theta\tan\theta]}{(\eta^2-1)(\eta^2-\tan^2\theta)}Q, \tag{20}$$

$$\Psi_{\mathrm{p}} = \mathrm{Re}\frac{\eta^2[\sqrt{\eta^2-\sin^2\theta} \mp \sin\theta\tan\theta]}{(\eta^2-1)(\eta^2-\tan^2\theta)}Q. \tag{21}$$

The polarization rotation and ellipticity of the LMOKE are given as follows, respectively.

$$\theta_{\mathrm{L}} = \mathrm{Im}\frac{\sin\theta\eta^2[\sqrt{\eta^2-\sin^2\theta} \pm \sin\theta\tan\theta]}{(\eta^2-1)(\eta^2-\tan^2\theta)\sqrt{\eta^2-\sin^2\theta}}Q, \tag{22}$$

$$\Psi_{\mathrm{L}} = \mathrm{Re}\frac{\sin\theta\eta^2[\sqrt{\eta^2-\sin^2\theta} \pm \sin\theta\tan\theta]}{(\eta^2-1)(\eta^2-\tan^2\theta)\sqrt{\eta^2-\sin^2\theta}}Q. \tag{23}$$

The reflectivity change of the TMOKE is

$$\delta_{\mathrm{T}} = \frac{I(M)-I(-M)}{I(0)} = -\mathrm{Im}\frac{4\tan\theta\eta^2}{(\eta^2-1)(\eta^2-\tan^2\theta)}Q, \tag{24}$$

where $\eta = n_2/n_1$ is the ratio of complex refractive index of the MO and reflective medium, θ is the incident angle, and $Q = g/\varepsilon_x$.

3 Typical magneto-optical materials

MO material refers to the functional material with MO effect, distinguished by the material attribute and applicable condition, such as metal/non-metallic, transparent/opaque, and its applicable wavelength and temperature range. Meanwhile, there are a variety of material forms, such as MO film, magnetic photonic crystal, MO glass, and magnetic liquid. The following presents the unique properties of the different types of materials.

FMs or alloy materials, such as Fe, Co, Ni, and NiFe, possess high MO coefficients at room temperature, i.e., the Faraday rotation angle per unit length. However, this cannot completely characterize the MO properties of the material in a transmitted system. The absorption must be considered. Since metals have high optical loss, the Faraday rotation normalized to attenuation is greatly reduced. Thus, they are more suitable for the reflective system. This type of MO material is usually processed by magnetron sputtering.

Non-metallic materials include three categories: garnet ferrite and its doped variants [19], high-conductivity semiconductor [20], and rare-earth compounds. Among them, garnet ferrite and its dopants are widely used in the visible and near-infrared since they have a relatively low optical loss at room temperature. The yttrium iron garnet (YIG) is transparent and exhibits a higher normalized Faraday rotation in the near-infrared but a lower absolute Faraday rotation. Therefore, if it is applied to a transmissive device, such as an isolator, a large size is required. Besides, its doped variants, such as Bi:YIG or Ce:YIG, are used to improve the MO response since the iron garnet has a relatively low Verdet constant. However, this type of material is more difficult to process, generally using the methods of radio frequency magnetron sputtering, liquid phase epitaxy (LPE), or pulsed laser deposition (PLD). Thus, it is necessary to explore a suitable process condition to achieve the thin-film deposition. It should be noted that the deposition rate is relatively slow, which takes several hours to obtain the microscale. A high-temperature annealing process is required to make it crystalline after the deposition. High-conductivity semiconductors include graphene, InSb, InAs, etc. Their carrier polarizations can be tuned by the external magnetic field, leading to the change of dielectric properties and MO phenomenon. They are generally processed by epitaxial growth and applied in the terahertz regime.

Rare-earth compounds include the Europium compounds [21], chromium compounds [22], or others, such as EuS, EuTe, EuO, CrI_3, $CrBr_3$, $CrCl_3$, and MnBi. They exhibit high transmittance and strong MO response at low temperature (below its Curie temperature, approximately several kelvins). Thus, they are more suitable for the transmitted system. Besides, their fabrication processes are relatively simple, generally using physical vapor deposition and are compatible with standard electron beam lithography. Hence, they are easier to be integrated with plasmonic nanostructures.

To summarize, typical MO materials can be classified according to the material type, processing technology, and application condition, as shown in Fig. 3. As for the fabrication process of the MO metasurfaces, it is generally performed by thin-film deposition combined with graphic process. Thin-film deposition processes include magnetron sputtering, thermal evaporation, atomic layer deposition, LPE, PLD, and so on. They are used to deposit the metal or dielectric thin films of the MO metasurfaces. Besides, electron beam lithography, ion beam etching, self-assembly, and other processes are used to pattern the nanostructure.

4 Magnetoplasmonic and magneto-optical metasurfaces

To enhance the response of MO material, a variety of strategies are proposed. One approach is to construct a Fabry-Perot cavity. By this way, the light energy is localized in the MO film layer due to its multiple reflections between the two interfaces of the cavity, which can enhance the MO effect. Another approach is to use localized surface plasmon (LSP), surface plasmon polariton (SPP), Mie resonance, or a combination of

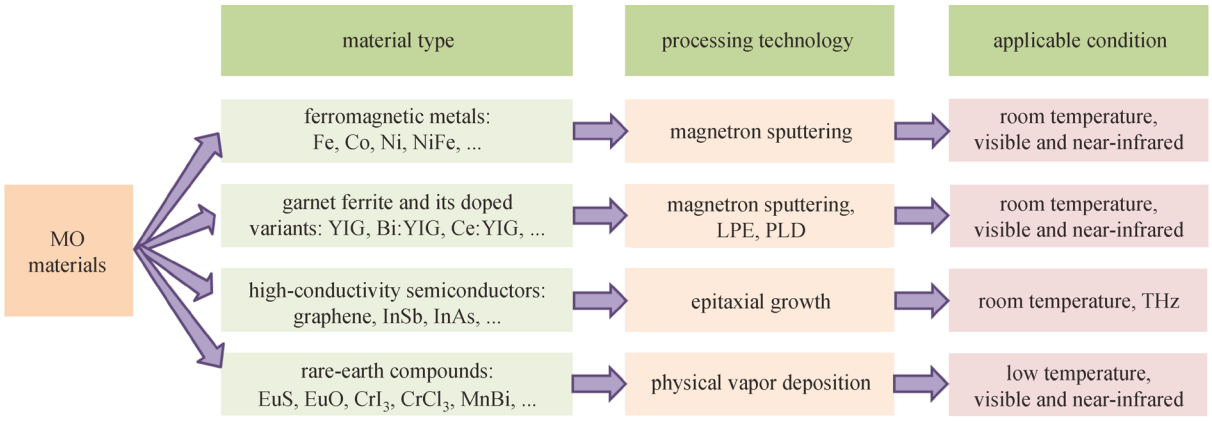

Fig. 3 Classification diagram of typical MO materials

multiple modes, such as Fano resonance and plasmon-waveguide mode coupling to generate a strong interaction between the light and MO medium to improve the MO performance. In the following, the existing magnetoplasmonic or MO nanostructures are classified according to the material composition, and the physical mechanism is also analyzed.

The magnetoplasmonic system based on FMs has attracted a lot of attentions since FMs have relatively large MO coefficient and strong plasmon resonance. In theory, Hui and Stroud predicted that the Faraday rotation enhancement occurred near the surface plasmon frequency of the metal particles [23]. This phenomenon results from the local electric field enhancement inside or on the surface of the nanoparticles. Then, researchers experimentally investigated the influence of local plasmon resonance on the MO response in the hexagonal Ni nanowire array embedded in the alumina template. Although the ratio of Ni nanowires only accounts for 15% of the bulk material, a polar Kerr angle of 0.15° equivalent to the bulk material was produced at 3.1 eV, as shown in Fig. 4(a) [24]. Moreover, the phase tunability of optical polarizability was realized by changing the size of the Ni nanodisk, which can produce the LSP and MO rotation simultaneously. The results showed that when the incident wavelength was 405 and 670 nm, and the diameter of the Ni nanodisk was 95 nm, the sign flip of LMOKE occurred, as shown in Fig. 4(b) [25]. The physical mechanism is that the resonance of the electrons in the nanodisk is in or out of phase with the exciting electric field when the resonant frequency is lower or higher than the LSP. Thus, the MO response derived from the action of Lorentz force will have a sign flip.

However, since FMs have high optical loss, their local resonance peaks are very wide, limiting the practical applications. Thus, researchers proposed some schemes. For example, Maccaferri et al. used the anisotropic Ni nanoantenna-based magnetoplasmonic crystal to effectively reduce the resonance peak width and achieve enhanced and tunable MO activity, as shown in Fig. 5(a) [26]. The coherent diffractive far-field coupling of the elliptical Ni nanoantenna derived from different plasma responses of the orthogonal axis to the incident field and the spin-orbit coupling caused by the external magnetic field. Besides, Chen et al. used the 2D Ni nanopillar array, which can simultaneously generate the LSP and SPP to realize narrow-band Fano resonance by proper structural design, as shown in Fig. 5(b) [27]. The tunable Fano

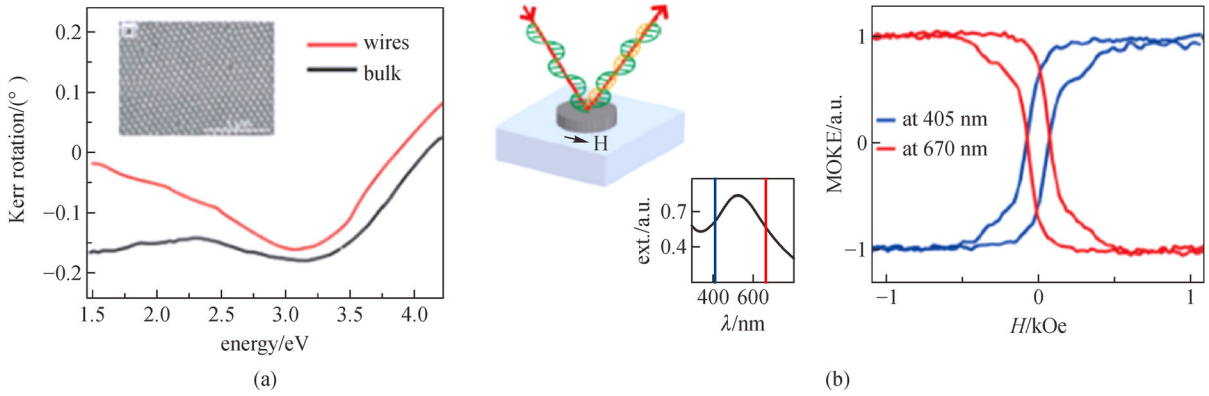

Fig. 4 (a) Kerr rotation of nickel nanowire array [24]. (b) Kerr sign reversal of nickel nanodisk [25]

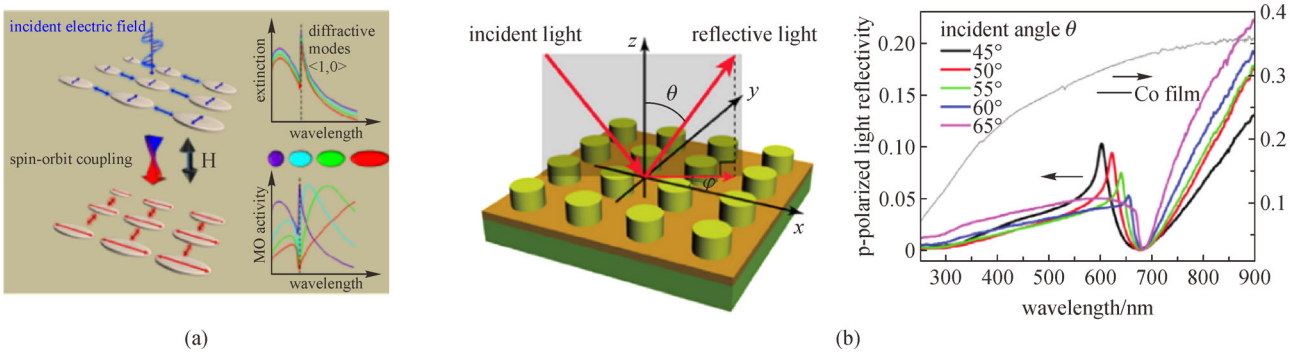

Fig. 5 (a) Enhanced and tunable MO activity of the anisotropic magnetoplasmonic crystal [26]. (b) Tunable Fano resonance and MO response in Ni nanopillars array [27]

resonance and MO response were realized by changing the azimuth of the incident p-polarized light. Additionally, similar 1D or 2D magnetoplasmonic metasurfaces, such as nanowires [28,29], nanoholes [30,31], or nanopillars [32,33], were also reported, and the manipulation of the transmitted or reflected polarization by the external magnetic field was studied.

Although FMs have higher MO coefficients in the visible and near-infrared, they also have higher optical loss. Whereas, NMs have lower optical loss and can be an alternative platform to support surface plasmon resonance (SPR). Thus, the better MO performance can be obtained based on the magnetoplasmonic system by combining the FM with NM. Li et al. studied the Faraday effect of dumbbell-like Ag-$CoFe_2O_4$ nanoparticle colloidal solution. They obtained that Ag-$CoFe_2O_4$ nanoparticle dimer had a higher Faraday rotation than $CoFe_2O_4$ monomer at a specific incident wavelength due to the effect of local plasmon resonance of Ag particles [34]. Subsequently, in the Au/Co/Au nanodisk sandwich structure [35], Ag-Fe alloy [36], and Ag-Co shell-like [37] nanostructures, the MO enhancement induced by the surface plasmon resonance was also observed. Therein, Wang et al. theoretically and experimentally proved the relationship between light absorption and MO effect in Ag-Co nanoparticles [37]. They also analyzed the interaction mechanism between plasmon resonance and MO activity in NM-FM. Meanwhile, Du et al. studied the effect of MO properties in the Au/CoPt/Au nanodisk by changing the geometric parameters [38]. In addition, it is worth mentioning that not only can the plasmon resonance of the metal be used to enhance the MO effect of the FMs in the magnetoplasmonic system [39–43], but the plasmon wave vector can also be modulated by the magnetic field [44–48]. Martín-Becerra et al. [49] demonstrated the manipulation of the real and imaginary parts of the surface plasmon resonance wave vector by the magnetic field in the Au/Co/Au sandwich structure covered with a dielectric layer polymethyl methacrylate (PMMA), as shown in Fig. 6.

Actually, the magnetoplasmonic system composed of NM-FM is not the only way to enhance the MO properties of the nanostructures. Researchers have demonstrated that the dielectric resonance can also enhance the MO response in FM-dielectric systems [50]. Barsukova et al. [51,52] found that the Faraday rotation reached 0.8° based on the MO metasurface composed of 5 nm thick Ni film deposited on the top layer of the amorphous Si nanopillars, which was five times stronger than the MO response of the pure Ni film. This phenomenon results from the local Mie resonance within the amorphous Si nanopillars, which supports electric and magnetic multipolar resonance modes, and the enhanced electric field interacts with the

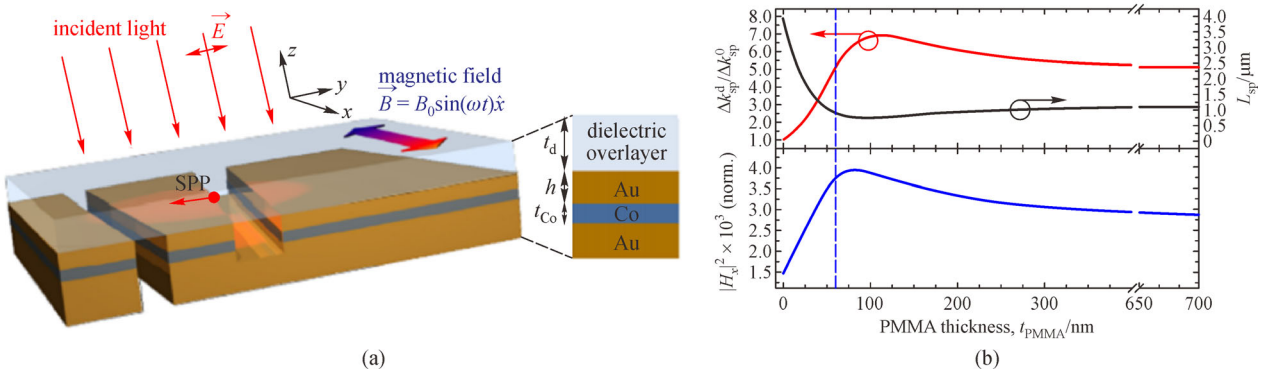

Fig. 6 (a) Sketch of the magnetoplasmonic structure of PMMA/Au/Co/Au. (b) SPR wave vector modulated by the magnetic field [49]

FM Ni to achieve enhancements of the MO response, as shown in Fig. 7(a). Moreover, Maccaferri et al. [53] realized the rotation increment of the LMOKE geometry composed of NiFe/Si magnetoplasmonic crystals that the cylindrical NiFe nanoholes were arranged on the Si substrate. The system showed the magneto-optically mediated coupling of SPP modes, and great enhancement of the MO response was induced when special noncollinear SPP modes were resonantly excited, as shown in Fig. 7(b).

Furthermore, considering the high optical loss of FM, which affects the modulation efficiency, researchers focused their attention on the low loss material system of ferromagnetic dielectric and NM. Belotelov's research group conducted many studies on the Kerr or Faraday effect of the metal-garnet or its doped variants from theory to experiment [54–57]. They studied the MO effect of the Au nanohole array/Bi:YIG film using the rigorous coupled-wave analysis, and found the enhanced Faraday and Kerr rotation near the resonance peak of the enhanced transmittance at the same time [58], as shown in Fig. 8(a). Compared with Bi:YIG thin film with the same thickness, the MO effect was increased by nine times. The physical mechanism was derived from the plasmon resonance of the metal/dielectric surface. It simultaneously satisfied the enhanced Faraday rotation and transmittance via the elaborate design of the structural parameters. In addition, they also studied the Faraday enhancement of the Au grating/BIG film, and the results showed that the coupling of the SPP mode excited by the grating and the waveguide mode in the magnetic dielectric would lead to the extraordinary optical transmission and enhancement of the MO activity [59,60]. The maximum rotation angle can be obtained by changing the magnetized SPP phase velocity, and the tunable resonance wavelength can be obtained by changing the grating period, as shown in Fig. 8(b).

Besides, the MO effect enhancement of 1D grating [61–64], and 2D nanoarray of different shapes [65,66] in similar physical mechanisms was also reported. In addition to the above mentioned metal/dielectric double-layer structure, the metal/dielectric/metal structure, such as Ag/Bi:YIG/Ag, could also realize the MO effect enhancement, and an asymmetric Fano resonance was found in the reflection spectrum of TMOKE signal [67]. The phenomenon was derived from the coupling of localized and propagating plasmon resonance modes to form the Fano resonance, leading to the enhancement of MO effect.

Compared with the above-mentioned MO nanostructures, all-dielectric MO metasurfaces [68–71] have the advantages of low optical loss, high Q value, and compatibility with CMOS technology, which have important research significance. In 2018, Christofi et al. [72] reported that an all-dielectric MO metasurface composed of BIG nanodisk array embedded in a low-refractive-index SiO_2 could achieve a giant enhancement of Faraday rotation. The MO enhancement was derived from the constructive interference of magnetic and electric dipole resonance, corresponding to the overlap of two resonance peaks of the transmission spectrum. It is called as the electromagnetically induced transparency, as shown in Fig. 9. Ignatyeva et al. [73] observed the intensity modulation of transparent all-dielectric MO metasurfaces composed of 2D nanopillar array on an ultrathin iron-garnet slab in a dual-polarization regime, which was very promising for sensing, vector magnetometer, and light modulation applications.

5 Application of magneto-optical metasurfaces

5.1 Nonreciprocal device

Nonreciprocal optical devices have important applications in the optical communication. At present, commercial optical isolators are usually based on Faraday effect. However, the fabrications are still challenging, and material costs are relatively high. Thus, it is urgent to realize integrated, compact, and low-cost nonreciprocal optical devices. To achieve the asymmetric transmission of nonreciprocal optical devices, it is necessary to break the

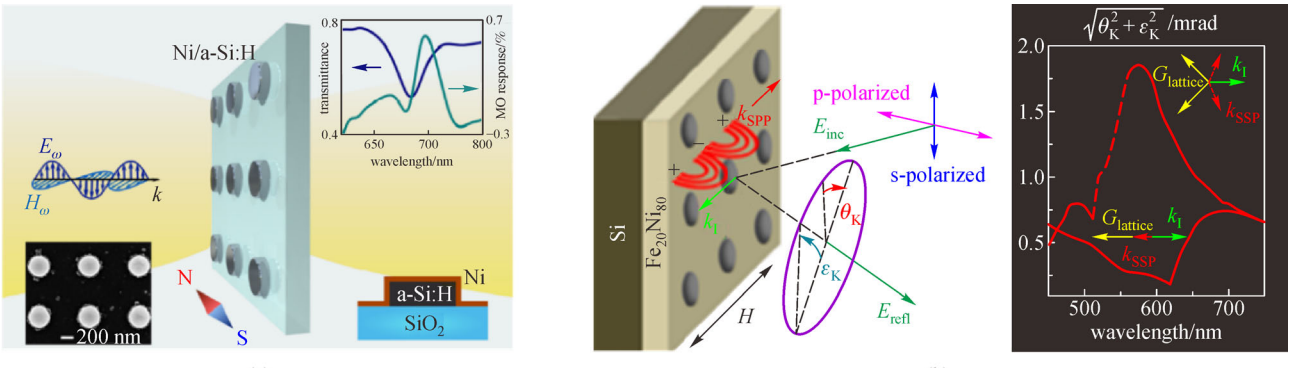

Fig. 7 (a) Enhanced MO response of the Ni-Si MO metasurface [51]. (b) Enhanced LMOKE of the anisotropic NiFe/Si magnetoplasmonic crystals [53]

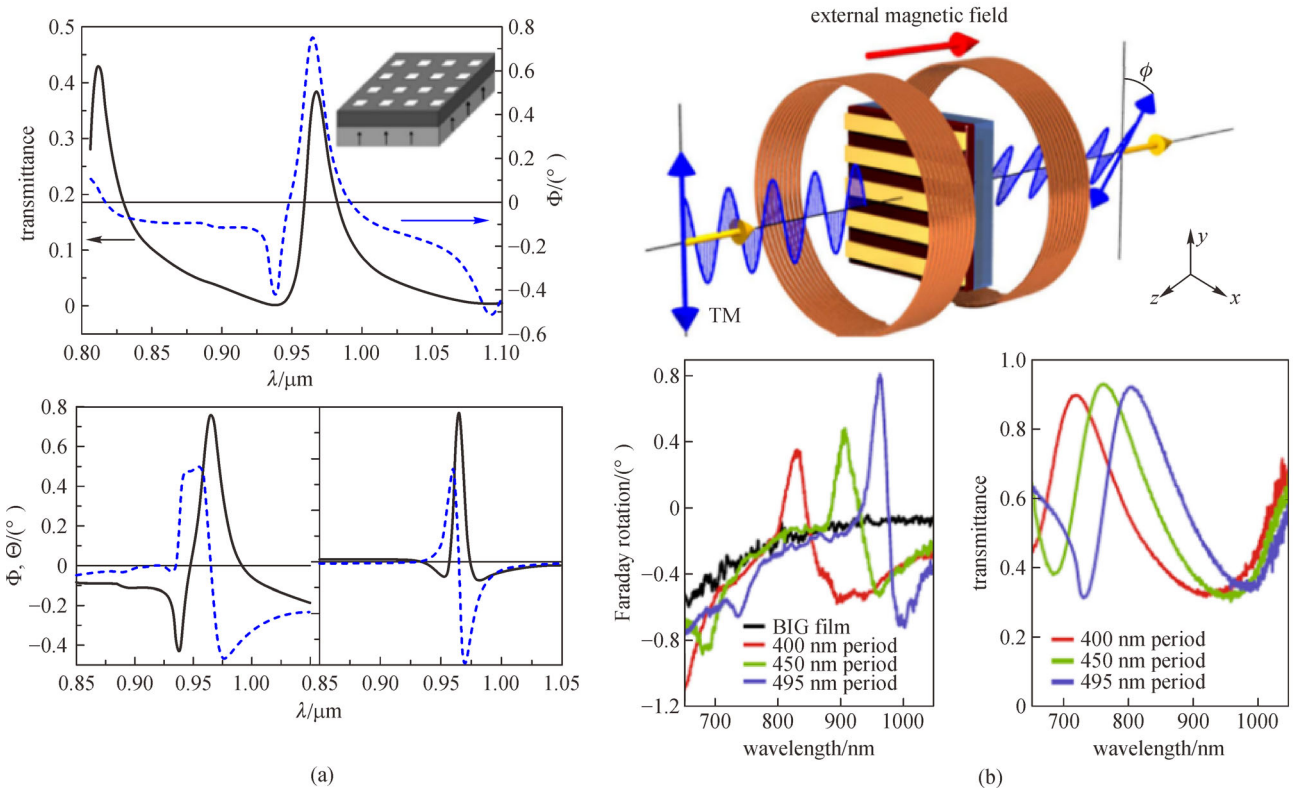

Fig. 8 (a) Transmission spectrum and MO effect of the Au nanohole array/Bi:YIG film [58]. (b) Tunable Faraday enhancement of Au grating/BIG film by changing the grating period [59]

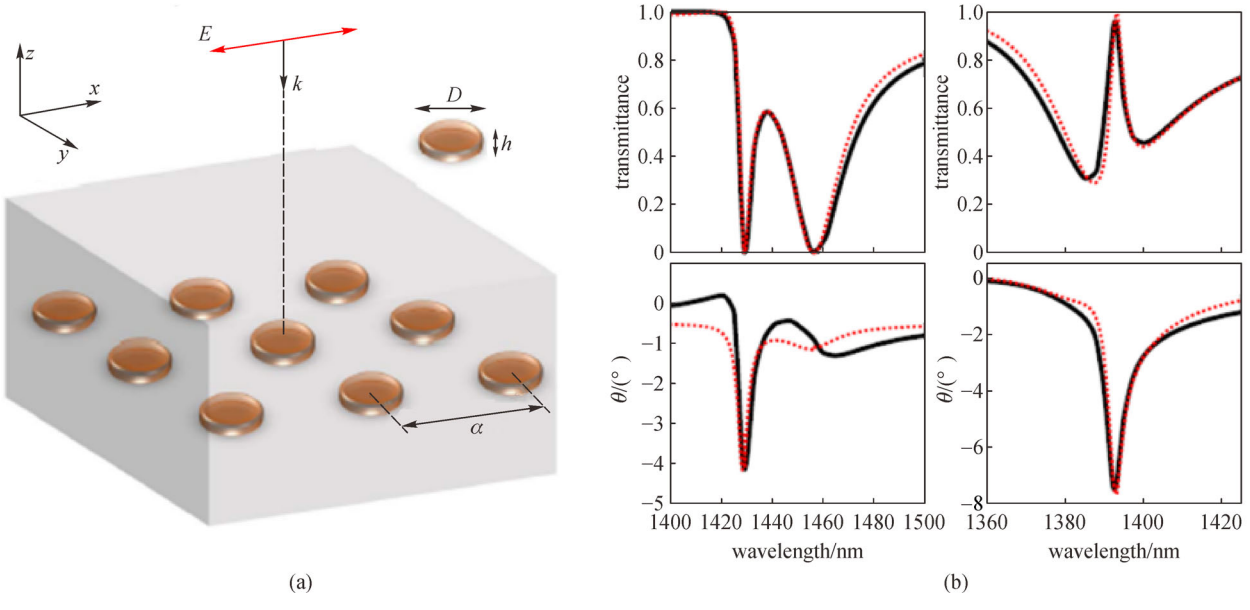

Fig. 9 (a) Structure of all-dielectric MO metasurface. (b) Transmittance spectra and Faraday rotation for the nonoverlapping and overlapping cases of the resonances [72]

Lorentz reciprocity. There are currently three technical approaches, that is using the nonlinear effect [74–76], dynamic spatial-temporal modulation (electrical or mechanical control) [77–79], and MO effect [80–83]. Although the first two methods have been reported, there are still some problems in device performance or integration process. For example, the bandwidth of nonlinear effect is generally narrow, and it requires strong laser energy. And dynamic spatial-temporal modulation requires complex external control circuits. However, the integrated nonreciprocal optical devices based on the MO effect have the advantages of passivity, broadband, and no need for an external circuit, which are very promising for applications.

The most primitive nonreciprocal device isolator was designed based on the Faraday effect. It was a separate block device, which consisted of a bulk MO material and two polarizers. The processing technology was particularly difficult, since the MO material, such as YIG, required to be hundreds of micrometers thick to achieve high-performance. Then, the first integrated MO nonreciprocal isolator device was performed by designing YIG or its dopant as a ridge waveguide. However, the light energy could not be completely converted between the two modes due to the phase mismatch of TM and TE orthogonal modes [84]. To overcome this problem, researchers proposed a variety of solutions, such as applying a periodic magnetic field or placing orthogonal MO materials. However, they all required extremely high phase matching accuracy, making the integration process be difficult. An integrated device based on the nonreciprocal phase shifting (NRPS) effect was proposed to break these limits. It involved that the forward and backward propagation constants of the TM mode were different when a magnetic field perpendicular to the light propagation was applied to the MO waveguide. Based on this principle, Auracher and Witte [85] proposed an interferometric MO isolator composed of two 3-dB couplers at the input and output of the device, which divided the input energy into two beams and modulated to a different phase. However, the NRPS effect of the MO waveguide was weak, and the device size required to be large enough.

Later, the tendency of MO devices need not only to be integrated, miniaturized, and low loss, but also be compatible with CMOS fabrication technique, to reduce device cost and improve device stability. Therefore, how to combine the MO material with semiconductor substrate became a new challenge. Shoji et al. [86] established a Mach-Zehnder interferometer (MZI) MO isolator by combining the MO material on the garnet with the III-V semiconductor substrate via wafer bonding. Additionally, Zhuromskyy et al. [87] proposed a silicon-based integrated isolation device scheme based on multimode interference (MMI), utilizing the characteristics of different NRPSs between modes in a multimode waveguide to achieve the asymmetry forward and backward transmission. Besides, Kono et al. [88] proposed an MO isolator based on the micro-ring resonator, which would produce different resonant wavelengths as the beam was propagating forward and backward if a radial magnetic field was applied to the micro-ring waveguide. Successively, many similar systems have been studied. Among these, the most prominent work was the one by Zhang et al. [89]. They experimentally demonstrated a monolithically integrated isolator with 19.5 dB isolation ratio at 1550 nm, as shown in Fig. 10. The working principle of this system was that the resonance frequency of the silicon ring resonator acting as notch filter depends on the light circulation direction.

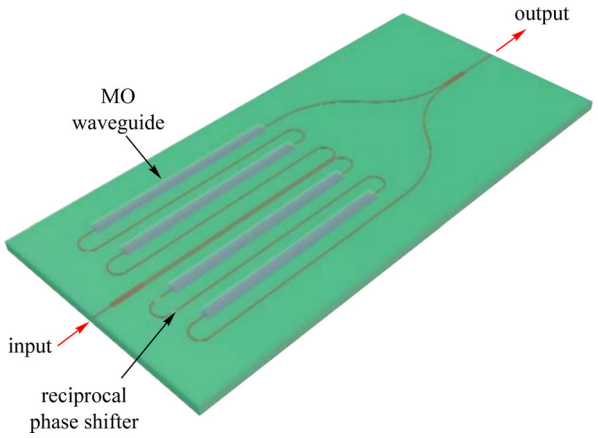

Fig. 10 Schematic of monolithically integrated MO isolator [89]

5.2 Sensing

In addition to nonreciprocal devices, sensing is another important application for MO metasurfaces, such as biochemical sensing, gas sensing, and chiral sensing. SPR is valuable in ultrasensitive biochemical detection due to its local field enhancement. Therefore, many MO metasurfaces combining SPR signal amplification have been proposed recently for biochemical and gas sensing [90–92]. The physical mechanism is that the enhanced local field caused by the SPR can increase the electro-magnetic field inside the adjacent MO layer. Importantly, TMOKE has the unique advantages of narrow peak width and high sensitivity to the surroundings. Thus, utilizing it to achieve SPR biochemical sensors can make the figure of merit (FOM) be greatly improved and the detection limit be reduced by three orders of magnitude.

However, SPR is generally required to be excited by prism coupling, which hinders the miniaturization of biochemical sensor devices. Thus, researchers proposed 1D or 2D grating coupling to achieve SPR excitation. For example, Diaz-Valencia et al. [93] proposed a simple structure that covered a 1D metal grating on the MO layer, as shown in Fig. 11(a). The high-sensitivity refractive

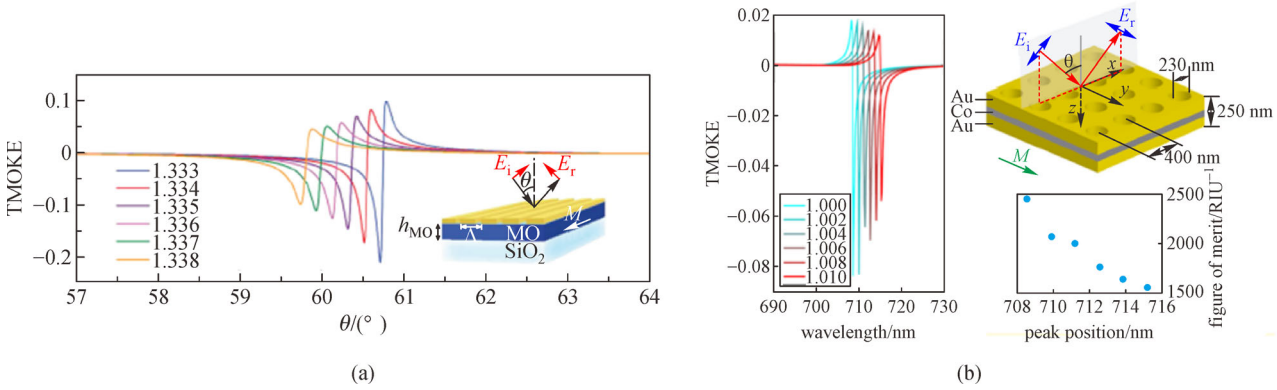

Fig. 11 (a) 1D grating/MO layer for refractive index sensing [93]. (b) Au/Co/Au magnetoplasmonic crystal for MOSPR sensor [94]

index sensing reaching 190 RIU^{-1} was realized based on the enhanced TMOKE. Moreover, Caballero et al. [94] proposed a novel MO surface plasmon resonance (MOSPR) sensor composed of Au/Co/Au magnetoplasmonic crystal with a 2D Au nanohole array on the top layer; it also realized enhanced sensing performance based on the measurement of TMOKE signal, as shown in Fig. 11(b). Compared with other SPR sensors, its FOM was improved by two orders of magnitude. Meanwhile, the sensing strategy using the nanohole structure has the advantages of miniaturization and facilitating combination with microfluidics to realize real-time biomolecule detection. Additionally, similar sandwich structures, such as Au/Fe/Au [95] and Ag/Co/Ag [96], have been widely applied to obtain excellent sensing performance by optimizing the film thickness of each layer. However, its main disadvantage is the need for highly precise nanoscale geometric fabrication. Thus, researchers proposed a simple multilayer plasma system to achieve the giant enhancement of TMOKE by using the epsilon-near-zero (ENZ) artificial metamaterial to exhibit new physical properties within a specific frequency range [97]. The system consisted of an indium tin oxide (ITO) ENZ thin film growing on a MO layer and a metal substrate. The SPR excitation can be achieved by matching the wave vector of ENZ mode generated by incident p-polarized light.

Additionally, large amounts of applications of MOSPR in biochemical sensors have emerged. For example, Rella and Manera [98] proposed a novel Au/Co/Au magnetoplasmonic nanostructure to achieve highly sensitive molecular detection. Zhang et al. [99] constructed a magnetoplasmonic nano detector based on FePt-Au nanorod, which applied magnetic field manipulation to perform optical imaging, drug delivery, real-time diagnosis, and treatment of single-molecule. Maccaferri et al. [100] utilized Ni nanodisks to implement a novel sensing application, which can achieve molecular-level detection of the polyamide by measuring the ellipticity change of transmitted and reflected light, as shown in Fig. 12. Pourjamal et al. [101] proved that the hybrid $Ni/SiO_2/Au$

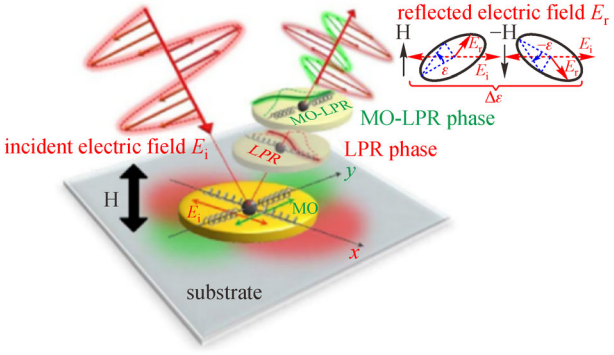

Fig. 12 MOSPR sensor based on Ni nanodisk [100]

dimer array had a higher sensitivity than the randomly distributed pure Ni nanodisks. In brief, sensors based on MOSPR have important applications in biochemical sensing, single-molecule sensing, and other fields. The main challenge currently exists is the relatively large optical loss of MO material, which limits the further improvement of the sensing performance. Therefore, it is necessary to propose some effective solutions, such as applying low loss material as the MO medium or introducing resonance response in the design of nanostructure.

Furthermore, MO metasurfaces can also be applied for chiral sensing. Eslami et al. [102] discovered the magneto-chiral dichroism in the Ni nanohelices. Subsequently, Armelles et al. [103] studied the magnetic field effect on the chiral response of 2D arrays of Au/Co multi-layered gammadions. It was found that the magnetoplasmonic structure had a larger chiro-optical response and magnetic field modulation at the resonant wavelength of 850 nm. Also, Zubritskaya et al. [104] used the Au-Au-Ni trimer nanoantennas to realize the magnetic control of the chiral response, and the magnetic field-induced modulation of the far-field chiroptical response exceeds 100% in the visible and near-infrared spectral ranges, as shown in Fig. 13(a).

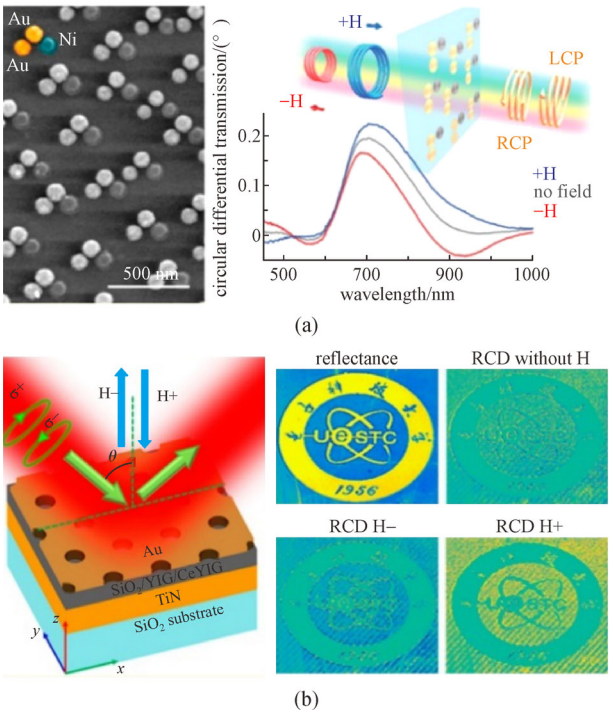

Fig. 13 (a) Magnetic control of the chiral response of Au-Au-Ni trimer [104]. (b) Switchable optical chirality in MO metasurfaces [105]

Besides, Qin et al. [105] adopted glancing incident condition to realize the giant and continuous far-field circular dichroism modulation from $-0.6\pm0.2°$ to $+1.9\pm0.1°$ by applying magnetic field to the achiral MO metasurfaces, as shown in Fig. 13(b). In a word, the chiral sensing of MO metasurfaces has important application value in the field of biomolecule detection.

6 Conclusions and future perspectives

In summary, magnetic field control provides an effective way to achieve tunable metasurfaces. So far, it faces the challenge of the weak coupling between the magnetic field and electromagnetic radiation, and the high loss of the MO materials. To overcome these challenges, researchers take many strategies that promise to open up a new path for future technologies, such as on-chip nanophotonics, ultrasensitive detection, all-optical technologies, and optical communications. Additionally, it should be noted that magnetophotonics may play a prominent role in the next generation of computer memory [106], as the hard drive industry faces a major challenge driven by the growing demand for data storage, that is, how to increase storage density further. Another important application of MO metasurfaces is using magnetic field manipulation to make nanoparticles play a role in medical diagnosis and drug delivery [107,108]. It was proved that the Au-Fe magnetic plasmonic nanoparticles have high sensitivity and resolution in magnetic resonance imaging (MRI), X-ray tomography (CT), and surface-enhanced Raman scattering (SERS) [109]. Moreover, it was reported that MO metasurfaces can function as magnetically tunable filters [110] and lenses [111]. The tunable filters were comprised of a single or cascaded H-shaped subwavelength resonant element made of magnetically controllable InAs in the terahertz regime. And the original concept of a tunable optical magnetic lens was put forward that focused photon beams using a graphene thin layer MO material in a non-uniform magnetic field. Importantly, MO metasurfaces are expected to have special phase profiles by elaborately structural design and be applied to some functional meta-devices in the future, such as beam steering or holograms. In short, it is necessary for magnetophotonic devices to put into practical that the magnetic spin manipulation of plasmons-assisted and the use of weak magnetic fields to achieve the interaction between light and nanoscale matter.

Acknowledgements The authors acknowledge the financial support from the National Key Research and Development Program of China (No. 2017YFB1002900), Fok Ying-Tong Education Foundation of China (No. 161009), the National Natural Science Foundation of China (Grant No. 61775019), and Beijing Outstanding Young Scientist Program (No. BJJWZYJH012019100070022).

Conflicts of interest The authors declare no conflict of interest.

References

1. Huang L, Chang C, Zeng B, Nogan J, Luo S N, Taylor A J, Azad A K, Chen H T. Bilayer metasurfaces for dual- and broadband optical

antireflection. ACS Photonics, 2017, 4(9): 2111–2116
2. Yu N, Genevet P, Kats M A, Aieta F, Tetienne J P, Capasso F, Gaburro Z. Light propagation with phase discontinuities: generalized laws of reflection and refraction. Science, 2011, 334(6054): 333–337
3. Liu Z, Li Z, Liu Z, Cheng H, Liu W, Tang C, Gu C, Li J, Chen H T, Chen S, Tian J. Single-layer plasmonic metasurface half-wave plates with wavelength-independent polarization conversion angle. ACS Photonics, 2017, 4(8): 2061–2069
4. Kim M, Wong A M, Eleftheriades G V. Optical huygens' metasurfaces with independent control of the magnitude and phase of the local reflection coefficients. Physical Review X, 2014, 4(4): 041042
5. Lee G Y, Yoon G, Lee S Y, Yun H, Cho J, Lee K, Kim H, Rho J, Lee B. Complete amplitude and phase control of light using broadband holographic metasurfaces. Nanoscale, 2018, 10(9): 4237–4245
6. Li J, Chen S, Yang H, Li J, Yu P, Cheng H, Gu C, Chen H T, Tian J. Simultaneous control of light polarization and phase distributions using plasmonic metasurfaces. Advanced Functional Materials, 2015, 25(5): 704–710
7. Ee H S, Agarwal R. Tunable metasurface and flat optical zoom lens on a stretchable substrate. Nano Letters, 2016, 16(4): 2818–2823
8. Cao T, Zhang L, Simpson R E, Wei C, Cryan M J. Strongly tunable circular dichroism in gammadion chiral phase-change metamaterials. Optics Express, 2013, 21(23): 27841–27851
9. Driscoll T, Palit S, Qazilbash M M, Brehm M, Keilmann F, Chae B G, Yun S J, Kim H T, Cho S Y, Jokerst N M, Smith D R, Basov D N. Dynamic tuning of an infrared hybrid-metamaterial resonance using vanadium dioxide. Applied Physics Letters, 2008, 93(2): 024101
10. Singh R, Azad A K, Jia Q X, Taylor A J, Chen H T. Thermal tunability in terahertz metamaterials fabricated on strontium titanate single-crystal substrates. Optics Letters, 2011, 36(7): 1230–1232
11. Goldflam M D, Liu M K, Chapler B C, Stinson H T, Sternbach A J, McLeod A S, Zhang J D, Geng K, Royal M, Kim B J, Averitt R D, Jokerst N M, Smith D R, Kim H T, Basov D N. Voltage switching of a VO_2 memory metasurface using ionic gel. Applied Physics Letters, 2014, 105(4): 041117
12. Ren M X, Wu W, Cai W, Pi B, Zhang X Z, Xu J J. Reconfigurable metasurfaces that enable light polarization control by light. Light, Science & Applications, 2017, 6(6): e16254
13. Yang H, Yu T, Wang Q, Lei M. Wave manipulation with magnetically tunable metasurfaces. Scientific Reports, 2017, 7(1): 5441
14. Armelles G, Cebollada A, Feng H Y, García-Martín A, Meneses-Rodríguez D, Zhao J, Giessen H. Interaction effects between magnetic and chiral building blocks: a new route for tunable magneto-chiral plasmonic structures. ACS Photonics, 2015, 2(9): 1272–1277
15. Ignatyeva D O, Knyazev G A, Kapralov P O, Dietler G, Sekatskii S K, Belotelov V I. Magneto-optical plasmonic heterostructure with ultranarrow resonance for sensing applications. Scientific Reports, 2016, 6(1): 28077
16. Knyazev G A, Kapralov P O, Gusev N A, Kalish A N, Vetoshko P M, Dagesyan S A, Shaposhnikov A N, Prokopov A R, Berzhansky V N, Zvezdin A K, Belotelov V I. Magnetoplasmonic crystals for highly sensitive magnetometry. ACS Photonics, 2018, 5(12): 4951–4959
17. Cheng F, Wang C, Su Z, Wang X, Cai Z, Sun N X, Liu Y. All-optical manipulation of magnetization in ferromagnetic thin films enhanced by plasmonic resonances. Nano Letters, 2020, 20(9): 6437–6443
18. Ho K S, Im S J, Pae J S, Ri C S, Han Y H, Herrmann J. Switchable plasmonic routers controlled by external magnetic fields by using magneto-plasmonic waveguides. Scientific Reports, 2018, 8(1): 10584
19. Wehlus T, Körner T, Leitenmeier S, Heinrich A, Stritzker B. Magneto-optical garnets for integrated optoelectronic devices. Physica Status Solidi, 2011, 208(2): 252–263
20. Yan H, Li Z, Li X, Zhu W, Avouris P, Xia F. Infrared spectroscopy of tunable Dirac terahertz magneto-plasmons in graphene. Nano Letters, 2012, 12(7): 3766–3771
21. Wachter P. Europium chalcogenides: EuO, EuS, EuSe and EuTe. Handbook on the Physics & Chemistry of Rare Earths, 1979, 2: 507–574
22. Huang B, Clark G, Navarro-Moratalla E, Klein D R, Cheng R, Seyler K L, Zhong D, Schmidgall E, McGuire M A, Cobden D H, Yao W, Xiao D, Jarillo-Herrero P, Xu X. Layer-dependent ferromagnetism in a van der Waals crystal down to the monolayer limit. Nature, 2017, 546(7657): 270–273
23. Hui P M, Stroud D. Theory of Faraday rotation by dilute suspensions of small particles. Applied Physics Letters, 1987, 50(15): 950–952
24. Melle S, Menéndez J L, Armelles G, Navas D, Vázquez M, Nielsch K, Wehrspohn R B, Gösele U. Magneto-optical properties of nickel nanowire arrays. Applied Physics Letters, 2003, 83(22): 4547–4549
25. Bonanni V, Bonetti S, Pakizeh T, Pirzadeh Z, Chen J, Nogués J, Vavassori P, Hillenbrand R, Åkerman J, Dmitriev A. Designer magnetoplasmonics with nickel nanoferromagnets. Nano Letters, 2011, 11(12): 5333–5338
26. Maccaferri N, Bergamini L, Pancaldi M, Schmidt M K, Kataja M, Dijken S, Zabala N, Aizpurua J, Vavassori P. Anisotropic nanoantenna-based magnetoplasmonic crystals for highly enhanced and tunable magneto-optical activity. Nano Letters, 2016, 16(4): 2533–2542
27. Chen L, Gao J, Xia W, Zhang S, Tang S, Zhang W, Li D, Wu X, Du Y. Tunable Fano resonance and magneto-optical response in magnetoplasmonic structure fabricated by pure ferromagnetic metals. Physical Review B, 2016, 93(21): 214411
28. González-Díaz J B, Garcia-Martin A, Armelles G, Navas D, Vázquez M, Nielsch K, Wehrspohn R B, Gösele U. Enhanced magneto-optics and size effects in ferromagnetic nanowire arrays. Advanced Materials, 2007, 19(18): 2643–2647
29. González-Díaz J B, García-Martín A, Reig G A. Unusual magneto-optical behavior induced by local dielectric variations under localized surface plasmon excitations. Nanoscale Research Letters, 2011, 6(1): 408
30. Ctistis G, Papaioannou E, Patoka P, Gutek J, Fumagalli P, Giersig

M. Optical and magnetic properties of hexagonal arrays of subwavelength holes in optically thin cobalt films. Nano Letters, 2009, 9(1): 1–6

31. Rollinger M, Thielen P, Melander E, Östman E, Kapaklis V, Obry B, Cinchetti M, García-Martín A, Aeschlimann M, Papaioannou E T. Light localization and magneto-optic enhancement in Ni antidot arrays. Nano Letters, 2016, 16(4): 2432–2438
32. Chen J, Albella P, Pirzadeh Z, Alonso-González P, Huth F, Bonetti S, Bonanni V, Åkerman J, Nogués J, Vavassori P, Dmitriev A, Aizpurua J, Hillenbrand R. Plasmonic nickel nanoantennas. Small, 2011, 7(16): 2341–2347
33. Kataja M, Hakala T K, Julku A, Huttunen M J, van Dijken S, Törmä P. Surface lattice resonances and magneto-optical response in magnetic nanoparticle arrays. Nature Communications, 2015, 6(1): 7072
34. Li Y, Zhang Q, Nurmikko A V, Sun S. Enhanced magnetooptical response in dumbbell-like Ag-$CoFe_2O_4$ nanoparticle pairs. Nano Letters, 2005, 5(9): 1689–1692
35. González-Díaz J B, García-Martín A, García-Martín J M, Cebollada A, Armelles G, Sepúlveda B, Alaverdyan Y, Käll M. Plasmonic Au/Co/Au nanosandwiches with enhanced magneto-optical activity. Small, 2008, 4(2): 202–205
36. Wang L, Yang K, Clavero C, Nelson A J, Carroll K J, Carpenter E E, Lukaszew R A. Localized surface plasmon resonance enhanced magneto-optical activity in core-shell Fe-Ag nanoparticles. Journal of Applied Physics, 2010, 107(9): 09B303
37. Wang L, Clavero C, Huba Z, Carroll K J, Carpenter E E, Gu D, Lukaszew R A. Plasmonics and enhanced magneto-optics in core-shell Co-Ag nanoparticles. Nano Letters, 2011, 11(3): 1237–1240
38. Du G X, Mori T, Suzuki M, Saito S, Fukuda H, Takahashi M. Magneto-optical effects in nanosandwich array with plasmonic structure of Au/[Co/Pt]n/Au. Journal of Applied Physics, 2010, 107(9): 09A928
39. Armelles G, González-Díaz J B, García-Martín A, García-Martín J M, Cebollada A, González M U, Acimovic S, Cesario J, Quidant R, Badenes G. Localized surface plasmon resonance effects on the magneto-optical activity of continuous Au/Co/Au trilayers. Optics Express, 2008, 16(20): 16104–16112
40. Armelles G, Cebollada A, García-Martín A, García-Martín J M, González M U, González-Díaz J B, Ferreiro-Vila E, Torrado J F. Magnetoplasmonic nanostructures: systems supporting both plasmonic and magnetic properties. Journal of Optics A, Pure and Applied Optics, 2009, 11(11): 114023
41. Du G X, Mori T, Suzuki M, Saito S, Fukuda H, Takahashi M. Evidence of localized surface plasmon enhanced magneto-optical effect in nanodisk array. Applied Physics Letters, 2010, 96(8): 081915
42. Du G X, Mori T, Saito S, Takahashi M. Shape-enhanced magneto-optical activity: degree of freedom for active plasmonics. Physical Review B: Condensed Matter, 2010, 82(16): 161403
43. Banthí J C, Meneses-Rodríguez D, García F, González M U, García-Martín A, Cebollada A, Armelles G. High magneto-optical activity and low optical losses in metal-dielectric Au/Co/Au-SiO_2 magnetoplasmonic nanodisks. Advanced Materials, 2012, 24(10): OP36–OP41
44. González-Díaz J B, García-Martín A, Armelles G, García-Martín J M, Clavero C, Cebollada A, Lukaszew R A, Skuza J R, Kumah D P, Clarke R. Surface-magnetoplasmon nonreciprocity effects in noble-metal/ferromagnetic heterostructures. Physical Review B, 2007, 76(15): 153402
45. Temnov V V, Armelles G, Woggon U, Guzatov D, Cebollada A, Garcia-Martin A, Garcia-Martin J M, Thomay T, Leitenstorfer A, Bratschitsch R. Active magneto-plasmonics in hybrid metal-ferromagnet structures. Nature Photonics, 2010, 4(2): 107–111
46. Clavero C, Yang K, Skuza J R, Lukaszew R A. Magnetic-field modulation of surface plasmon polaritons on gratings. Optics Letters, 2010, 35(10): 1557–1559
47. Martín-Becerra D, Temnov V V, Thomay T, Leitenstorfer A, Bratschitsch R, Armelles G, García-Martín A, González M U. Spectral dependence of the magnetic modulation of surface plasmon polaritons in noble/ferromagnetic/noble metal films. Physical Review B, 2012, 86(3): 035118
48. Jung I, Jang H J, Han S, Acapulco J A I Jr, Park S. Magnetic modulation of surface plasmon resonance by tailoring magnetically responsive metallic block in multisegment nanorods. Chemistry of Materials, 2015, 27(24): 8433–8441
49. Martín-Becerra D, González-Díaz J B, Temnov V V, Cebollada A, Armelles G, Thomay T, Leitenstorfer A, Bratschitsch R, García-Martín A, González M U. Enhancement of the magnetic modulation of surface plasmon polaritons in Au/Co/Au films. Applied Physics Letters, 2010, 97(18): 183114
50. Lu Y H, Cho M H, Kim J B, Lee G J, Lee Y P, Rhee J Y. Magneto-optical enhancement through gyrotropic gratings. Optics Express, 2008, 16(8): 5378–5384
51. Barsukova M G, Shorokhov A S, Musorin A I, Neshev D N, Kivshar Y S, Fedyanin A A. Magneto-optical response enhanced by Mie resonances in nanoantennas. ACS Photonics, 2017, 4(10): 2390–2395
52. Barsukova M G, Musorin A I, Shorokhov A S, Fedyanin A A. Enhanced magneto-optical effects in hybrid Ni-Si metasurfaces. APL Photonics, 2019, 4(1): 016102
53. Maccaferri N, Inchausti X, García-Martín A, Cuevas J C, Tripathy D, Adeyeye A O, Vavassori P. Resonant enhancement of magneto-optical activity induced by surface plasmon polariton modes coupling in 2D magnetoplasmonic crystals. ACS Photonics, 2015, 2(12): 1769–1779
54. Belotelov V I, Bykov D A, Doskolovich L L, Kalish A N, Kotov V A, Zvezdin A K. Giant magneto-optical orientational effect in plasmonic heterostructures. Optics Letters, 2009, 34(4): 398–400
55. Belotelov V I, Kreilkamp L E, Akimov I A, Kalish A N, Bykov D A, Kasture S, Yallapragada V J, Venu Gopal A, Grishin A M, Khartsev S I, Nur-E-Alam M, Vasiliev M, Doskolovich L L, Yakovlev D R, Alameh K, Zvezdin A K, Bayer M. Plasmon-mediated magneto-optical transparency. Nature Communications, 2013, 4(1): 2128
56. Borovkova O, Kalish A, Belotelov V. Transverse magneto-optical Kerr effect in active magneto-plasmonic structures. Optics Letters, 2016, 41(19): 4593–4596
57. Kalish A N, Komarov R S, Kozhaev M A, Achanta V G, Dagesyan S A, Shaposhnikov A N, Prokopov A R, Berzhansky V N, Zvezdin A K, Belotelov V I. Magnetoplasmonic quasicrystals: an approach for multiband magneto-optical response. Optica, 2018, 5(5): 617

58. Belotelov V I, Doskolovich L L, Zvezdin A K. Extraordinary magneto-optical effects and transmission through metal-dielectric plasmonic systems. Physical Review Letters, 2007, 98(7): 077401
59. Chin J Y, Steinle T, Wehlus T, Dregely D, Weiss T, Belotelov V I, Stritzker B, Giessen H. Nonreciprocal plasmonics enables giant enhancement of thin-film Faraday rotation. Nature Communications, 2013, 4(1): 1599
60. Kreilkamp L E, Belotelov V I, Chin J Y, Neutzner S, Dregely D, Wehlus T, Akimov I A, Bayer M, Stritzker B, Giessen H. Waveguide-plasmon polaritons enhance transverse magneto-optical Kerr effect. Physical Review X, 2013, 3(4): 041019
61. Belotelov V I, Doskolovich L L, Kotov V A, Bezus E A, Bykov D A, Zvezdin A K. Magnetooptical effects in the metal-dielectric gratings. Optics Communications, 2007, 278(1): 104–109
62. Belotelov V I, Bykov D A, Doskolovich L L, Kalish A N, Zvezdin A K. Extraordinary transmission and giant magneto-optical transverse Kerr effect in plasmonic nanostructured films. Journal of the Optical Society of America B, Optical Physics, 2009, 26(8): 1594–1598
63. Halagačka L, Vanwolleghem M, Postava K, Dagens B, Pištora J. Coupled mode enhanced giant magnetoplasmonics transverse Kerr effect. Optics Express, 2013, 21(19): 21741–21755
64. Dyakov S A, Fradkin I M, Gippius N A, Klompmaker L, Spitzer F, Yalcin E, Akimov I A, Bayer M, Yavsin D A, Pavlov S I, Pevtsov A B, Verbin S Y, Tikhodeev S G. Wide band enhancement of transverse magneto-optic Kerr effect in magnetite-based plasmonic crystals. Physical Review B: Condensed Matter, 2019, 100(21): 214411
65. Wang Y, Qin Y, Zhang Z. Extraordinary optical transmission property of X-shaped plasmonic nanohole arrays. Plasmonics, 2014, 9(2): 203–207
66. Li D, Lei C, Chen L, Tang Z, Zhang S, Tang S, Du Y. Waveguide plasmon resonance induced enhancement of the magneto-optics in a Ag/Bi:YIG bilayer structure. Journal of the Optical Society of America B, Optical Physics, 2015, 32(9): 2003
67. Chesnitskiy A V, Gayduk A E, Prinz V Y. Transverse magneto-optical Kerr effect in strongly coupled plasmon gratings. Plasmonics, 2018, 13(3): 885–889
68. Gamet E, Varghese B, Verrier I, Royer F. Enhancement of magneto-optical effects by a single 1D all dielectric resonant grating. Journal of Physics D, Applied Physics, 2017, 50(49): 495105
69. Levy M, Borovkova O V, Sheidler C, Blasiola B, Karki D, Jomard F, Kozhaev M A, Popova E, Keller N, Belotelov V I. Faraday rotation in iron garnet films beyond elemental substitutions. Optica, 2019, 6(5): 642
70. Royer F, Varghese B, Gamet E, Neveu S, Jourlin Y, Jamon D. Enhancement of both Faraday and Kerr effects with an all-dielectric grating based on a magneto-optical nanocomposite material. ACS Omega, 2020, 5(6): 2886–2892
71. Moncada-Villa E, Mejía-Salazar J R. High-refractive-index materials for giant enhancement of the transverse magneto-optical Kerr effect. Sensors (Basel), 2020, 20(4): 952
72. Christofi A, Kawaguchi Y, Alù A, Khanikaev A B. Giant enhancement of Faraday rotation due to electromagnetically induced transparency in all-dielectric magneto-optical metasurfaces. Optics Letters, 2018, 43(8): 1838–1841
73. Ignatyeva D O, Karki D, Voronov A A, Kozhaev M A, Krichevsky D M, Chernov A I, Levy M, Belotelov V I. All-dielectric magnetic metasurface for advanced light control in dual polarizations combined with high-Q resonances. Nature Communications, 2020, 11(1): 5487
74. Fan L, Wang J, Varghese L T, Shen H, Niu B, Xuan Y, Weiner A M, Qi M. An all-silicon passive optical diode. Science, 2012, 335 (6067): 447–450
75. Shi Y, Yu Z, Fan S. Limitations of nonlinear optical isolators due to dynamic reciprocity. Nature Photonics, 2015, 9(6): 388–392
76. Peng B, Özdemir Ş K, Lei F, Monifi F, Gianfreda M, Long G L, Fan S, Nori F, Bender C M, Yang L. Parity–time-symmetric whispering-gallery microcavities. Nature Physics, 2014, 10(5): 394–398
77. Doerr C R, Chen L, Vermeulen D. Silicon photonics broadband modulation-based isolator. Optics Express, 2014, 22(4): 4493–4498
78. Sounas D L, Alù A. Non-reciprocal photonics based on time modulation. Nature Photonics, 2017, 11(12): 774–783
79. Sohn D B, Kim S, Bahl G. Time-reversal symmetry breaking with acoustic pumping of nanophotonic circuits. Nature Photonics, 2018, 12(2): 91–97
80. Zhang C, Dulal P, Stadler B J H, Hutchings D C. Monolithically-integrated TE-mode 1D silicon-on-insulator isolators using seedlayer-free garnet. Scientific Reports, 2017, 7(1): 5820
81. Chen R, Tao D, Zhou H, Hao Y, Yang J, Wang M, Jiang X. Asymmetric multimode interference isolator based on nonreciprocal phase shift. Optics Communications, 2009, 282(5): 862–866
82. Huang D, Pintus P, Shoji Y, Morton P, Mizumoto T, Bowers J E. Integrated broadband Ce:YIG/Si Mach-Zehnder optical isolators with over 100 nm tuning range. Optics Letters, 2017, 42(23): 4901–4904
83. Liu N, Zhao J, Du L, Niu C, Sun C, Kong X, Wang Z, Li X. Giant nonreciprocal transmission in low-biased gyrotropic metasurfaces. Optics Letters, 2020, 45(21): 5917–5920
84. Liu Q, Gross S, Dekker P, Withford M J, Steel M J. Competition of Faraday rotation and birefringence in femtosecond laser direct written waveguides in magneto-optical glass. Optics Express, 2014, 22(23): 28037–28051
85. Auracher F, Witte H H. A new design for an integrated optical isolator. Optics Communications, 1975, 13(4): 435–438
86. Shoji Y, Mizumoto T, Yokoi H, Hsieh I W, Osgood R M Jr. Magneto-optical isolator with silicon waveguides fabricated by direct bonding. Applied Physics Letters, 2008, 92(7): 071117
87. Zhuromskyy O, Lohmeyer M, Bahlmann N, Hertel P, Dötsch H, Popkov A F. Analysis of nonreciprocal light propagation in multimode imaging devices. Optical and Quantum Electronics, 2000, 32(6–8): 885–897
88. Kono N, Kakihara K, Saitoh K, Koshiba M. Nonreciprocal microresonators for the miniaturization of optical waveguide isolators. Optics Express, 2007, 15(12): 7737–7751
89. Zhang Y, Du Q, Wang C, Fakhrul T, Liu S, Deng L, Huang D, Pintus P, Bowers J, Ross C A, Hu J, Bi L. Monolithic integration of

broadband optical isolators for polarization-diverse silicon photonics. Optica, 2019, 6(4): 473–478
90. Regatos D, Sepúlveda B, Fariña D, Carrascosa L G, Lechuga L M. Suitable combination of noble/ferromagnetic metal multilayers for enhanced magneto-plasmonic biosensing. Optics Express, 2011, 19(9): 8336–8346
91. Manera M G, Ferreiro-Vila E, García-Martín J M, Cebollada A, García-Martín A, Giancane G, Valli L, Rella R. Enhanced magneto-optical SPR platform for amine sensing based on Zn porphyrin dimers. Sensors and Actuators B, Chemical, 2013, 182: 232–238
92. Ignatyeva D O, Knyazev G A, Kapralov P O, Dietler G, Sekatskii S K, Belotelov V I. Magneto-optical plasmonic heterostructure with ultranarrow resonance for sensing applications. Scientific Reports, 2016, 6(1): 28077
93. Diaz-Valencia B F, Mejía-Salazar J R, Oliveira O N Jr, Porras-Montenegro N, Albella P. Enhanced transverse magneto optical Kerr effect in magnetoplasmonic crystals for the design of highly sensitive plasmonic (bio)sensing patforms. ACS Omega, 2017, 2(11): 7682–7685
94. Caballero B, García-Martín A, Cuevas J C. Hybrid magnetoplasmonic crystals boost the performance of nanohole arrays as plasmonic sensors. ACS Photonics, 2016, 3(2): 203–208
95. Regatos D, Fariña D, Calle A, Cebollada A, Sepúlveda B, Armelles G, Lechuga L M. Au/Fe/Au multilayer transducers for magneto-optic surface plasmon resonance sensing. Journal of Applied Physics, 2010, 108(5): 054502
96. Ferreiro-Vila E, Gonzalez-Diaz J B, Fermento R, González M U, García-Martín A, García-Martín J M, Cebollada A, Armelles G, Meneses-Rodríguez D, Sandoval E M. Intertwined magneto-optical and plasmonic effects in Ag/Co/Ag layered structures. Physical Review B, 2009, 80(12): 125132
97. Traviss D, Bruck R, Mills B, Abb M, Muskens O L. Ultrafast plasmonics using transparent conductive oxide hybrids in the epsilon-near-zero regime. Applied Physics Letters, 2013, 102(12): 121112
98. Rella R, Manera M G. Magneto-optical modulation for improved surface plasmon resonance sensors. SPIE Professional, 2016
99. Zhang Y, Wang Q, Ashall B, Zerulla D, Lee G U. Magnetic-plasmonic dual modulated FePt-Au ternary heterostructured nanorods as a promising nano-bioprobe. Advanced Materials, 2012, 24(18): 2485–2490
100. Maccaferri N, Gregorczyk K E, de Oliveira T V, Kataja M, van Dijken S, Pirzadeh Z, Dmitriev A, Åkerman J, Knez M, Vavassori P. Ultrasensitive and label-free molecular-level detection enabled by light phase control in magnetoplasmonic nanoantennas. Nature Communications, 2015, 6(1): 6150
101. Pourjamal S, Kataja M, Maccaferri N, Vavassori P, van Dijken S. Hybrid Ni/SiO_2/Au dimer arrays for high-resolution refractive index sensing. Nanophotonics, 2018, 7(5): 905–912
102. Eslami S, Gibbs J G, Rechkemmer Y, van Slageren J, Alarcón-Correa M, Lee T C, Mark A G, Rikken G L J A, Fischer P. Chiral Nanomagnets. ACS Photonics, 2014, 1(11): 1231–1236
103. Armelles G, Caballero B, Prieto P, García F, Cebollada A, González M U, García-Martin A. Magnetic field modulation of chirooptical effects in magnetoplasmonic structures. Nanoscale, 2014, 6(7): 3737–3741
104. Zubritskaya I, Maccaferri N, Inchausti Ezeiza X, Vavassori P, Dmitriev A. Magnetic control of the chiroptical plasmonic surfaces. Nano Letters, 2018, 18(1): 302–307
105. Qin J, Deng L, Kang T, Nie L, Feng H, Wang H, Yang R, Liang X, Tang T, Shen J, Li C, Wang H, Luo Y, Armelles G, Bi L. Switching the optical chirality in magnetoplasmonic metasurfaces using applied magnetic fields. ACS Nano, 2020, 14(3): 2808–2816
106. Stipe B, Strand T, Poon C, Balamane H, Boone T D, Katine J A, Li J L, Rawat V, Nemoto H, Hirotsune A, Hellwig O, Ruiz R, Dobisz E, Kercher D S, Robertson N, Albrecht T R, Terris B D. Magnetic recording at 1.5 Pb m^{-2} using an integrated plasmonic antenna. Nature Photonics, 2010, 4(7): 484–488
107. Zhang Y, Wang Q, Ashall B, Zerulla D, Lee G U. Magnetic-plasmonic dual modulated FePt-Au ternary heterostructured nanorods as a promising nano-bioprobe. Advanced materials, 2012, 24(18): 2485–2490
108. Vetoshko P M, Gusev N A, Chepurnova D A, Samoilova E V, Zvezdin A K, Korotaeva A A, Belotelov V I. Rat magnetocardiography using a flux-gate sensor based on iron garnet films. Biomedical Engineering, 2016, 50(4): 237–240
109. Amendola V, Scaramuzza S, Litti L, Meneghetti M, Zuccolotto G, Rosato A, Nicolato E, Marzola P, Fracasso G, Anselmi C, Pinto M, Colombatti M. Magneto-plasmonic Au-Fe alloy nanoparticles designed for multimodal SERS-MRI-CT imaging. Small, 2014, 10 (12): 2476–2486
110. Serebryannikov A E, Lakhtakia A, Ozbay E. Single and cascaded, magnetically controllable metasurfaces as terahertz filters. Journal of the Optical Society of America B, Optical Physics, 2016, 33(5): 834–841
111. Shamuilov G, Domina K, Khardikov V, Nikitin A, Goryashko V. Optical magnetic lens: towards actively tunable terahertz optics. Nanoscale, 2021, 13: 108–116

Yu Bi received her B.E. degree in Communication Engineering from North University of China, China, in 2013. After that, she took a successive master-doctor combined program at North University and received her Ph.D. degree in Instrument Science and Technology, in 2019. Currently she is a postdoctoral fellow at Beijing Institute of Technology, China. Her research focuses on magneto-optical metasurfaces and micro-nano magnetic sensor.

Lingling Huang received her Double B.S. degree (both Science and Engineering B.S. degree) in Optoelectronics from Tianjin University and Nankai University, China, in 2009. And she received her Ph.D. degree in Optical Engineering from Tsinghua University, China, in 2014. Currently she is a professor in Beijing Institute of Technology, China. Her research activities are focused on nanophotonics and optical metasurfaces.

Xiaowei Li received his bachelor's degree from Huazhong University of Science and Technology, China, in 2006. Then, he received his Ph.D. degree from Department of Precision Instruments and Mechanics, Tsinghua University, China, in 2012. Currently he is a professor in Beijing Institute of Technology and work as a director of Laser Micro/Nano-Fabrication Laboratory, China. His research focuses on micro-nano laser fabrication methods and their applications.

Yongtian Wang received his B.E. degree from Department of Precision Instrument, Tianjin University, China, in 1981 and his Ph.D. degree in Physics from Reading University, UK, in 1986. Currently he is a professor in Beijing Institute of Technology, China. His research focuses on the design of novel optical components and system, virtual reality and augmented reality, and medical image processing.